Supplementary Materials for

Title: New molecular probes reveal callose structural diversity in plant cell wall microdomains

Authors: Sam Amsbury[1], Susan E. Marcus[2], Richa Yeshvekar[2], Jenny Barber[2], Liam German[2†], James F. Ross[3], Ieva Lelenaite[4], Tatiana de Souza Moraes[5], Janithri Wickramanayake[6], Anastasiya Klebanovych[6], Brandon C. Reagan[7≠], Kirk Czymmek[6], Tessa M. Burch-Smith[8], Emmanuelle M. Bayer[5], William Willats[4], Iain W. Manfield[3], Paul Knox[2], Yoselin Benitez-Alfonso[2,3]*

Corresponding author: y.benitez-alfonso@leeds.ac.uk

The PDF file includes:

Figs. S1 to S10
Table S1, S2

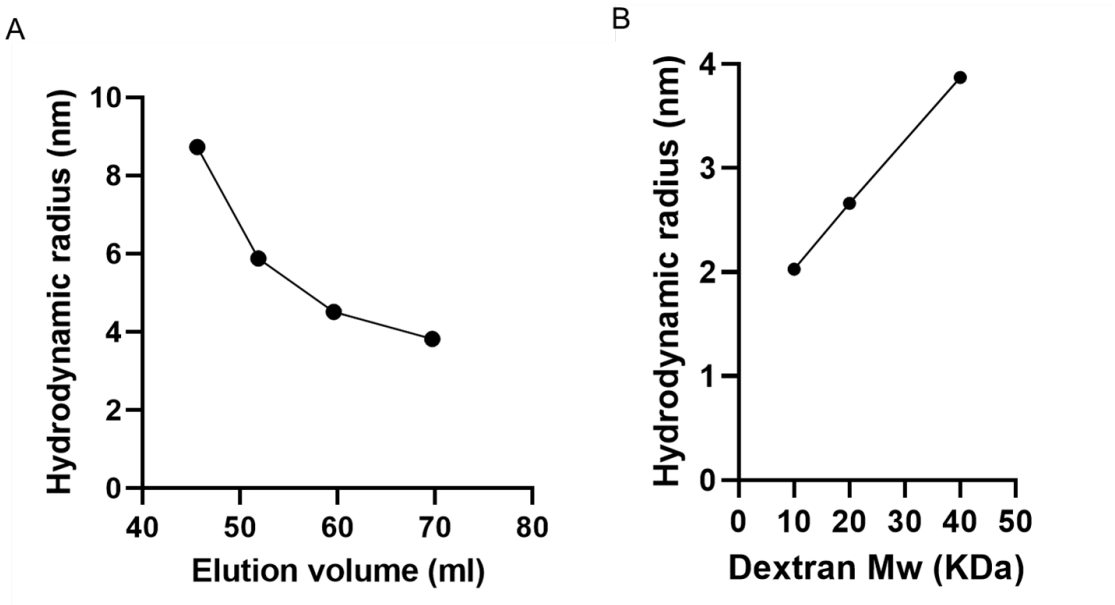

Fig. S1. Size exclusion separation of standards. (A) Size exclusion chromatography was carried out using thyroglobulin, ferritin, aldolase and conalbumin protein standards (669, 440, 158 and 75 kDa respectively). Elution volume vs hydrodynamic radius (determined using FIDA) is represented. **(B)** The hydrodynamic radius of dextran standards were calculated using FIDA and plotted against their MW. A 40 kDa dextran has a hydrodynamic radius of 3.87 nm equivalent to a protein with elution volume of ~70 ml and similar MW as Pachyman.

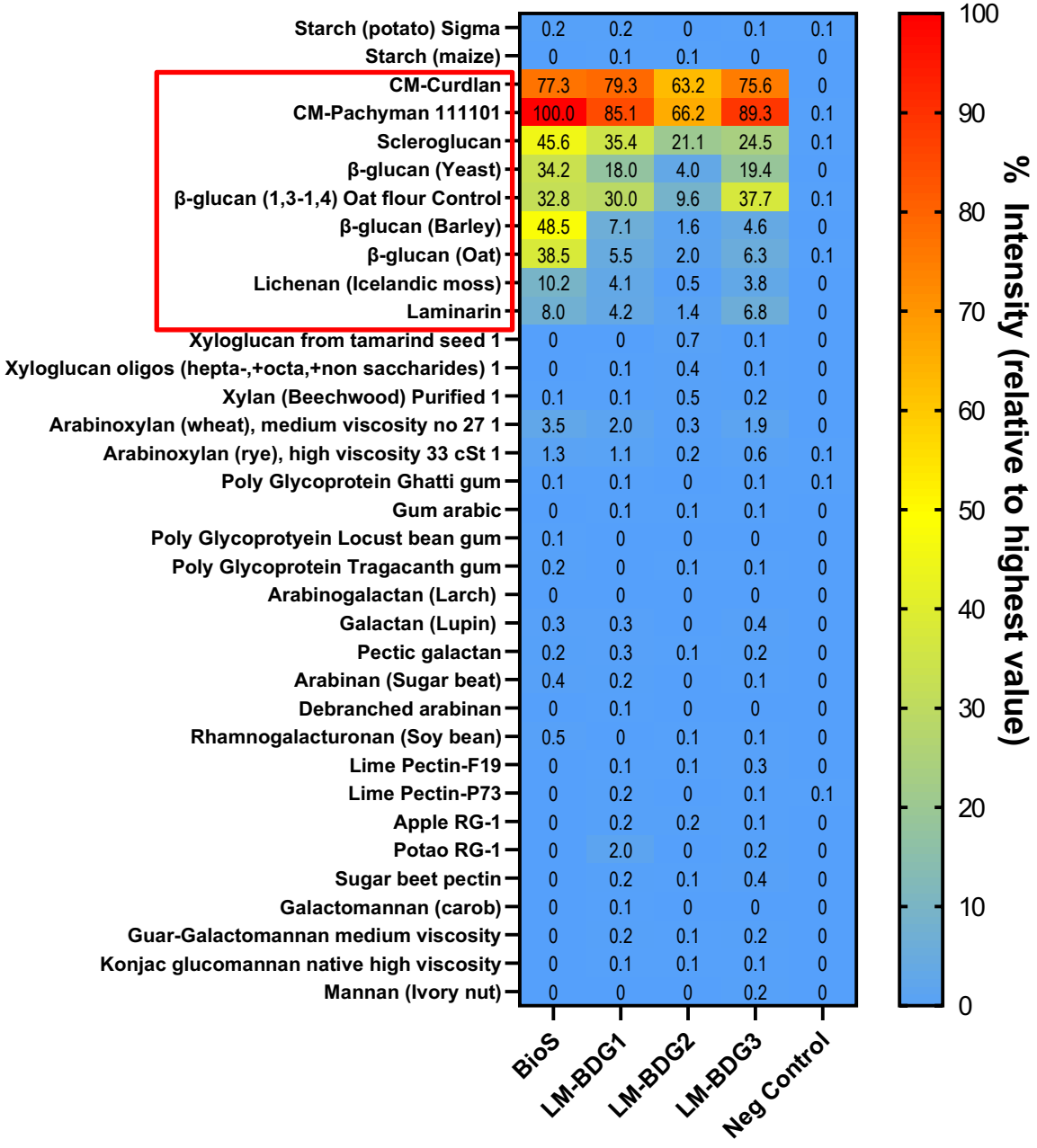

Fig. S2. Glycomicroarray of callose monoclonal antibodies against polysaccharide standards. The intensity of the signal relative to the highest value was calculated and presented from low (blue) to high (red) in the table. Commercial substrates with β-(1,3)-glucan linkages are indicated in the red box (including mixed linkage glucans). No substantial binding was observed in components that do not contain β-(1,3)-glucan linkages. Affinity was highest against pachyman and curdlan. BioS has significant binding to mixed linkage glucans which was not observed with LM-BDG2. LM-BDG1 and LM-BDG3 have similar specificity.

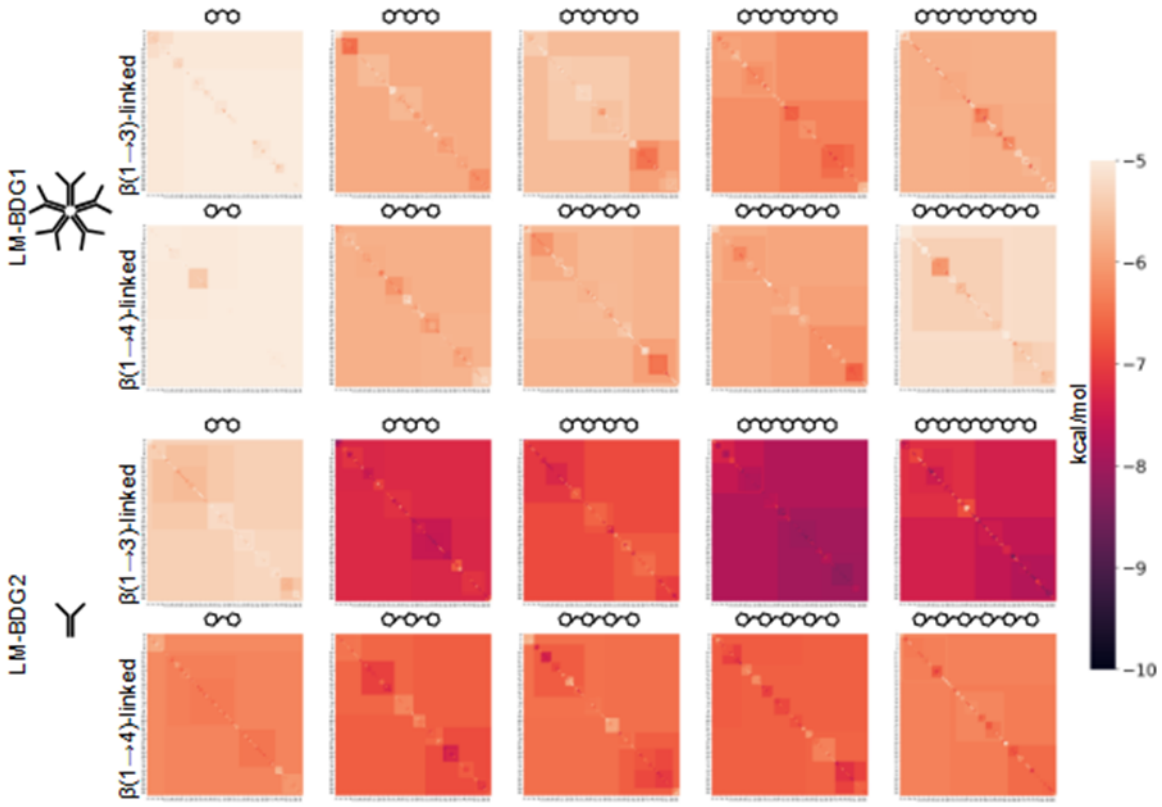

Fig. S3. Vinacarb docking energy landscapes. Vinacarb was used to dock β-(1-3) and β-(1-4) linked saccharides of 2-6 glucose residues in length to the LM-BDG1 and LM-BDG2 antigen-binding site. Pairwise RMSD values were calculated between the docked poses of 90 sugar molecules for each experiment. A clustered RMSD matrix was generated with hierarchical clustering to identify groups of structurally similar docked conformations. For each resulting cluster, the predicted binding free energies (kcal·mol^{-1}) of all member sugars were averaged. These cluster-averaged binding energies are overlaid onto the RMSD matrix, allowing the relationship between structural similarity and docking energetics to be visualised.

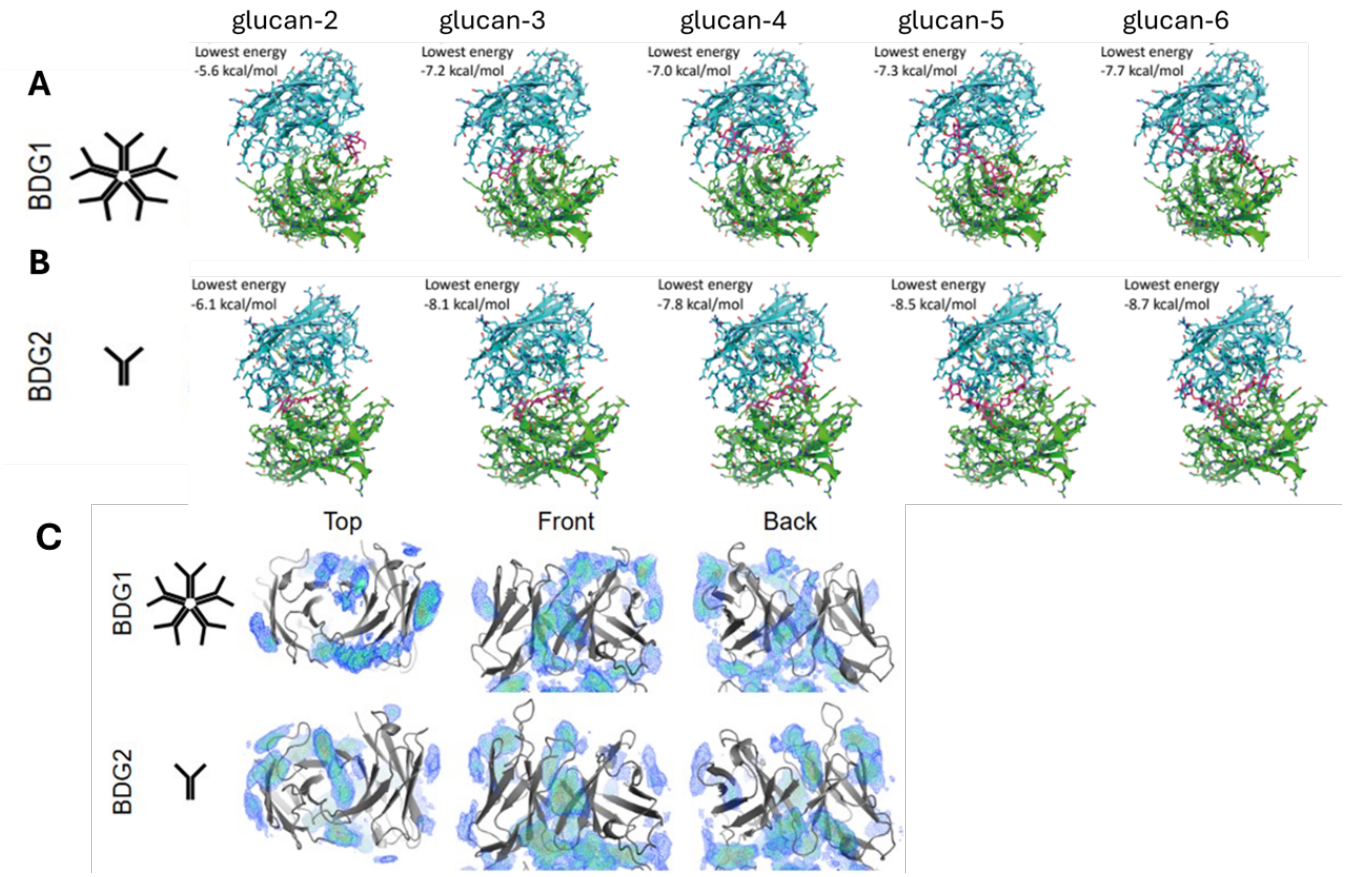

Fig. S4. BDG1 and BDG2 docking and co-solvent simulations with β(1-3)-linked glucans. **A**) LM-BDG1 and **B**) LM-BDG2 binding clefts with beta-1-3 glucan oligomers of 2, 3, 4, 5 and 6 residues docked with Vina-Carb. The lowest energy structure (according to Fig. S3) is depicted (antibody in blue and green, glucan in magenta) with interaction energy stated (kcal/mol). **C**) BDG1 and BDG2 (variable fragments) structures co-simulated with high concentrations of diglucose (laminaribiose), representing Laminarin-like chains. For each protein, ten independent 1 μs simulations were performed, with each simulation containing ~56 disaccharide molecules. Repulsive intermolecular interactions between disaccharides were introduced to prevent sugar–sugar aggregation and to promote independent sampling of protein–sugar interactions. Atomic density maps of disaccharide positions were then calculated and averaged across the ten replicate simulations. The resulting contoured density maps represent regions of high spatial occupancy, indicating preferred and recurrent disaccharide binding locations on the protein surface. In the above images, LM-BDG2 show increased high-density binding (red) in the classical Ab binding groove and surrounding areas, LM-BDG1 shows more widespread lower density (dark-blue) interactions.

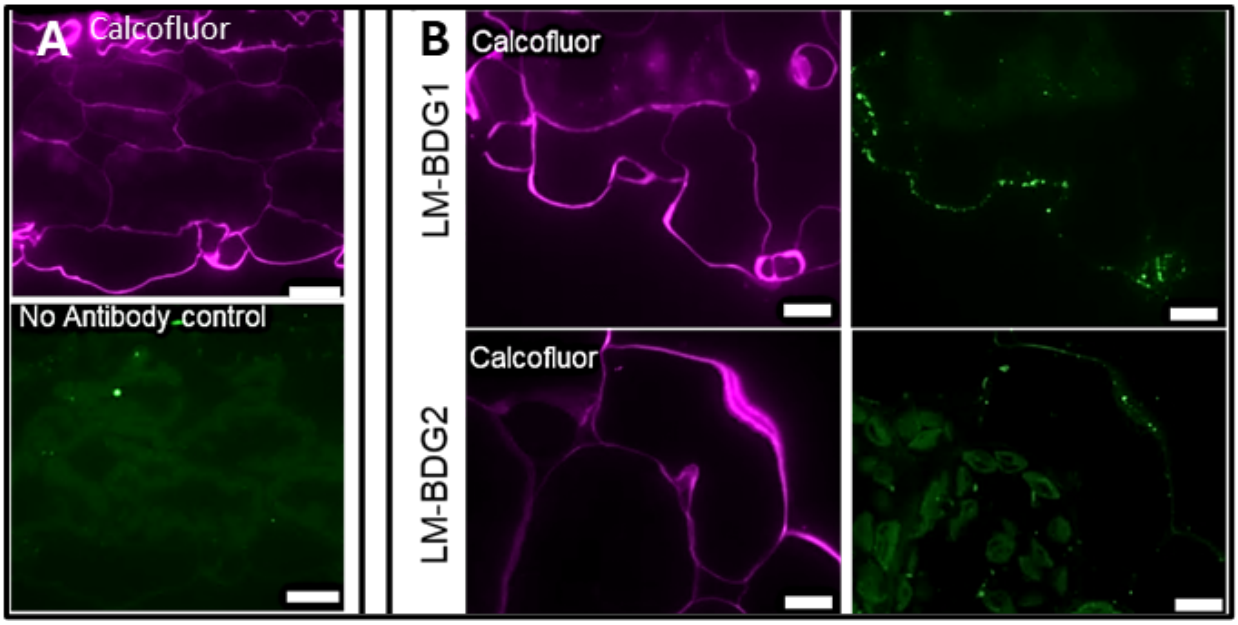

Fig. S5. Fluorescent immunolabelling of Arabidopsis leaf sections. (A) No-primary antibody controls for Arabidopsis wildtype Col-0 presented in Fig. 3 to capture autofluorescence. **(B)** Wildtype (WT) Arabidopsis leaf section labelled with LM-BDG1 and LM-BDG2 showing presence of both epitopes in cell walls. Counterstaining of cellulose with calcofluor white shown in magenta. Scale bars = 20 µm

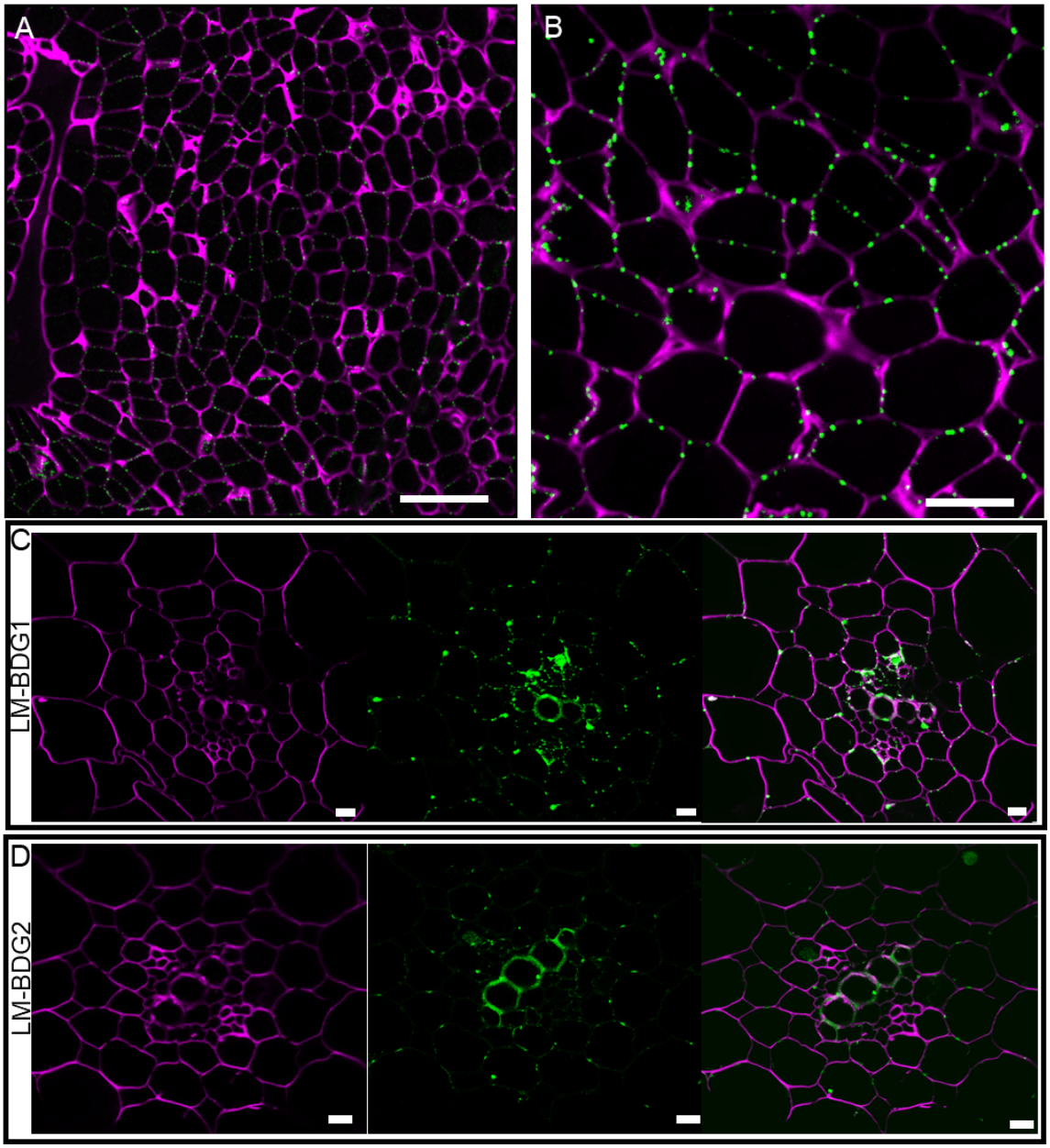

Fig. S6. Immunofluorescence detection of callose in aspen and tobacco tissues. (A, B) Immunofluorescence in the shoot apical meristem of Aspen Hybrid T89 using LM-BDG1 and detected with a secondary antibody conjugated with anti-rat-AlexaFluor-555 (green)**. (C, D)** Tobacco root sections were labelled with LM-BDG1 and LM-BDG2 and revealed using anti-rat-Alexa-488 (green). Labelling showed presence of both LM-BDG1 (**C**) and LM-BDG2 (**D**). Counterstaining of cellulose with calcofluor white is shown in magenta. Scale bars = 20 µm (A, **C, D**) and 5 µm (**B**).

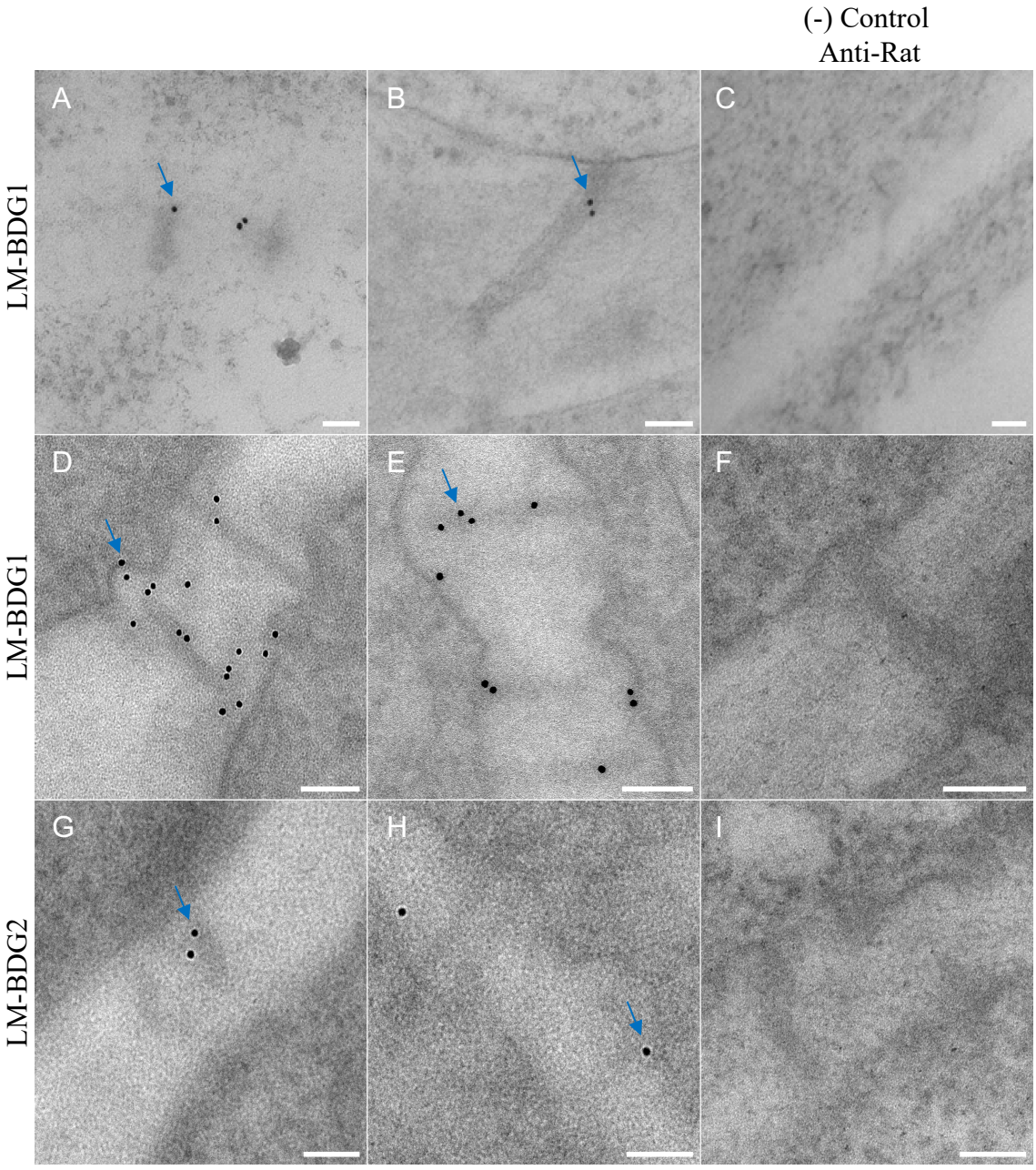

Fig S7. Immunogold TEM labelling callose in Arabidopsis cell cultures and aspen buds. Immunogold EM labelling showed gold-labelled callose (blue arrows, **A-B, D-E, F-G**) detected by LM-BDG1 at plasmodesmata compared to absence of labelling in representative Rat non-immune IgG controls (**C, F, I**). Sections from Arabidopsis culture cells (**A-C**) and the meristem region of Aspen Hybrid T89 (**D-I**) are shown. Scale bar = 100 nm.

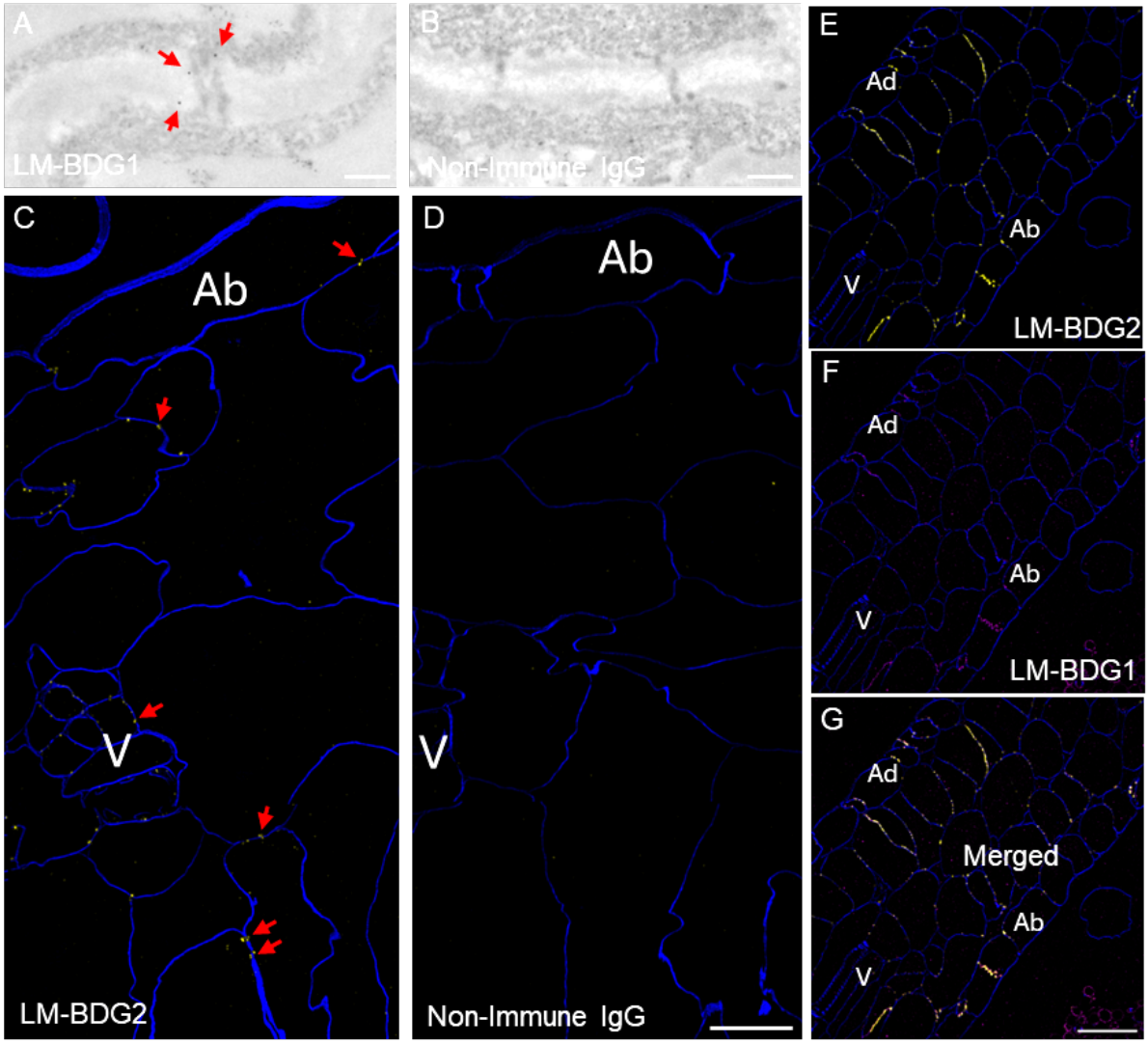

Fig S8. Immunogold TEM and multiplex immunofluorescence Lattice SIM2 super-resolution microscopy of callose at plasmodesmata (overviews and non-immune controls). (**A-B**) Immunogold EM labelling in tobacco leaf sections showed gold-labelled callose (red arrows) was detected by LM-BDG1 at plasmodesmata compared to absence of labelling in representative Rat non-immune IgG controls. Scale bar = 200nm. (**C-D**) Tiled large area overview immunofluorescence localization of LM-BDG2 (yellow) at plasmodesmata (red arrows) (**C**) and absence of specific labelling with non-immune Rat IgG negative control (**D**). Calcofluor White cell wall counterstain (blue), adaxial epidermis (Ad), vascular tissue (V). **C** & **D** leaf sections acquired using SIM2 super-resolution microscopy from same samples as Fig. 3 **C-G** and displayed with matched acquisition and brightness contrast settings. Scale bar = 10µm. (**E-G**) Overview Lattice SIM2 super-resolution microscopy immunofluorescence of LM-BDG2 (yellow) and LM-BDG1 (magenta) at plasmodesmata showed some localization overlap and non-overlap adjacency of signals. Calcofluor white cell wall counterstain (blue), adaxial epidermis (Ad), abaxial epidermis (Ab), vascular tissue (V). Scale bar = 20µm.

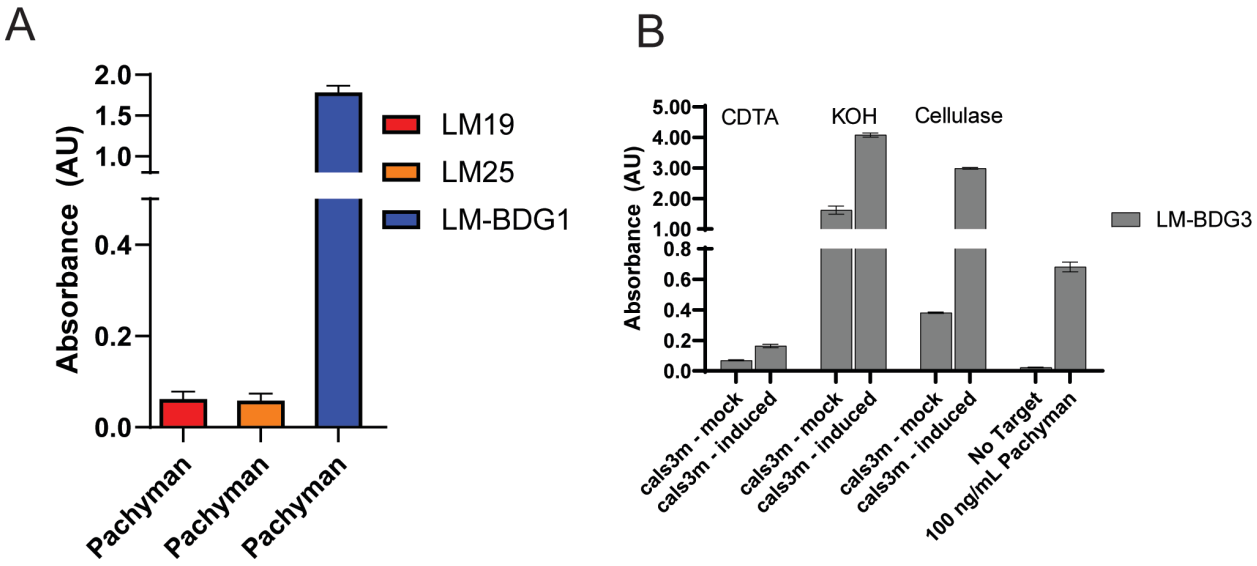

Fig S9. Sandwich ELISA control experiments. (A) Control experiments carried out using a callose-binding module (CBM43) to capture Pachyman indicate no binding of LM19 (pectin mAb) or LM25 (xyloglucan mAb) but strong signal when using LM-BDG1. Error bars represent standard deviation from n=4 pools of 4 plants each. (**B**) To confirm callose immuno-detection by LM-BDG1-HRP, sandwich ELISA were also carried out using LM-BDG3 as a capture antibody. Increases in calloses by i*cals3m* were observed in all extracts. Pachyman was used as positive control. Error bars show standard error (SEM) from n=3. Statistical significance: *** indicates $p<0.005$ *** indicates $p<0.0005$ determined by 2-way ANOVA.

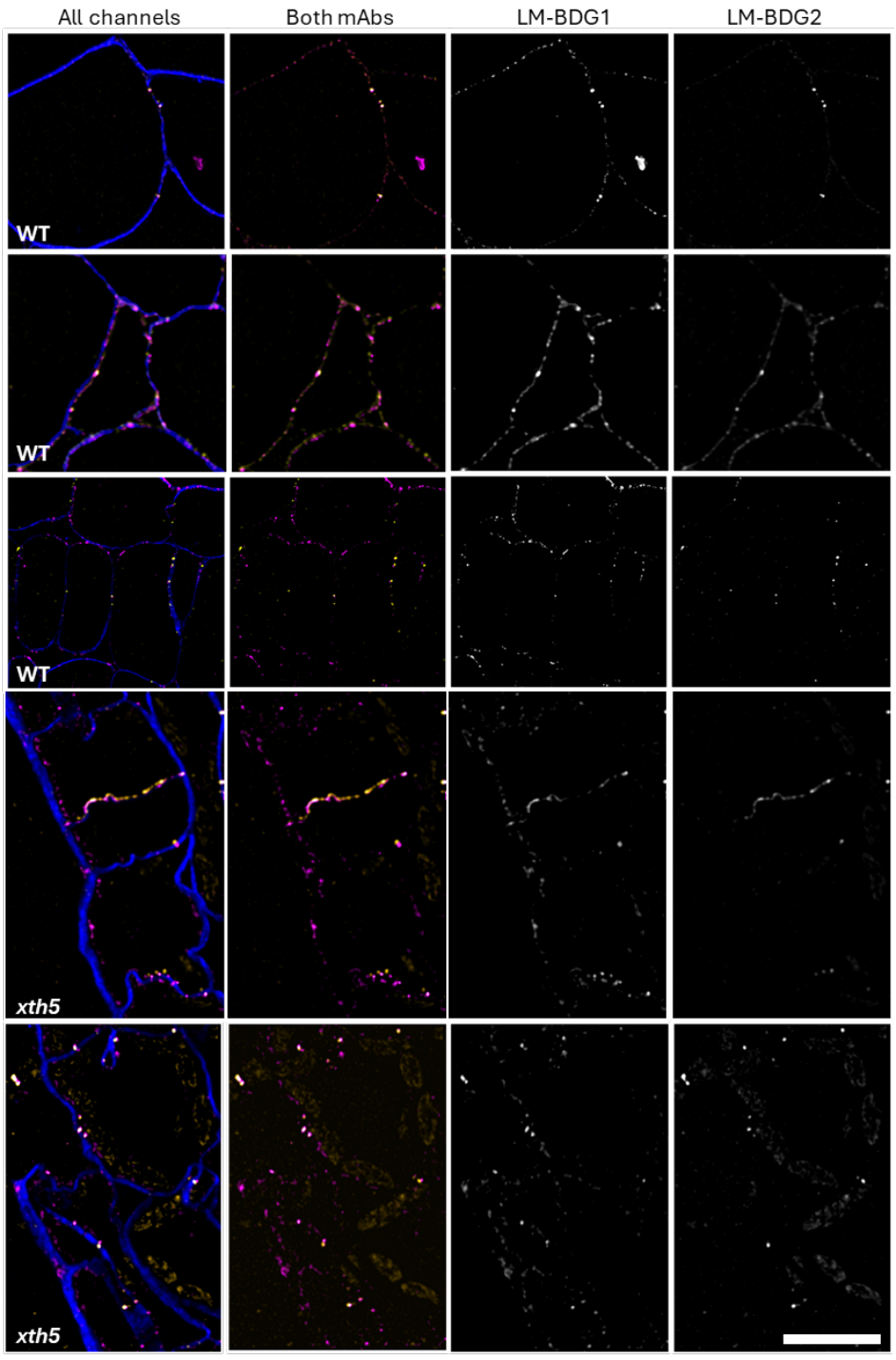

Fig S10. Multiplex immunofluorescence Lattice SIM2 super-resolution microscopy of callose in XTH5 VIGS *(xth5*) and WT controls. Lattice SIM2 super-resolution microscopy immunofluorescence of LM-BDG1 and LM-BDG2 at plasmodesmata. When both antibodies are present LM-BDG1 is in magenta and LM-BDG2 in yellow, when presented

individually (columns 3 and 4) antibodies remain in their captured greyscale. Calcofluor white cell wall counterstain appears in blue. LM-BDG1 is in magenta and LM-BDG2 in yellow when both antibodies are present. Scale bar = 20μm.

Table S1. *N. benthamiana XTH* sequences silenced and the corresponding gene ID from the Nicomics database (http://lifenglab.hzau.edu.cn/Nicomics/)

XTH name	Nb Gene ID
NbXTH1	*Nbe06g00090*
NbXTH2	*Nbe07g26330.1*
NbXTH3	*Nbe04g25650.1*
NbXTH4	*Nbe03g11800.1*
NbXTH5	*1Nbe13g36880.1*

Table S2. Primers used for generating VIGS constructs targeting *NbXTH* genes.

Name	Sequence	Purpose
XTH1F	ATCGGATCCGGTTGAATGAAGAGTTAG	Forward primer for *XTH1* into pYL156
XTH1R	CCGCTCGAGCTAGTTGGTACAAAAC	Reverse primer for *XTH1* into pYL156
XTH2F	CTAGGATCCGAGATTGATGGCTGTGAATG	Forward primer for *XTH2* into pYL156
XTH2R	GATCTCGAGCAAGCAGAGGCAACAGATG	Reverse primer for *XTH2* into pYL156
XTH3F	AAAGAATTCGATATTACATGGGGTGAT	Forward primer for *XTH3* into pYL156
XTH3R	TTTTCTAGACTGCTCTCTATTTCCTTTCCCTT	Reverse primer for *XTH3* into pYL156
XTH4F	TACGGATCCCTGTGCCTCAAATCCACGC	Forward primer for *XTH4* into pYL156
XTH4R	CGACTCGAGCAATATATTACAGCAATAAG	Reverse primer for *XTH4* into pYL156
XTH5F	AAAGAATTCGGCATGTGCATATCTCCGTTA	Forward primer for *XTH5* into pYL156
XTH5R	TTTTCTAGACACCCATGGTGAAAGTTCTAAAG	Reverse primer for *XTH5* into pYL156